"ANOMALOUS EM SIGNALS AND CHANGES IN RESISTIVITY AT PARKFIELD: COLLABORATIVE RESEARCH BETWEEN THE UNIVERSITIES OF CALIFORNIA AT BERKELEY AND RIVERSIDE AND OREGON STATE UNIVERSITY"

FINAL REPORT FOR JANUARY, 2004- JANUARY, 2005
APRIL, 2007

STEPHEN PARK
University of California, Riverside
The Institute of Geophysics and Planetary Physics
Riverside, California 92521
(951)-827-4501;(951)-827-4324(fax)
magneto@ucrmt.ucr.edu

Submitted to:

UNITED STATES DEPARTMENT OF THE INTERIOR
GEOLOGICAL SURVEY
NATIONAL EARTHQUAKE HAZARDS REDUCTION PROGRAM

Grant 04HQGR0061

"ANOMALOUS EM SIGNALS AND CHANGES IN RESISTIVITY AT PARKFIELD: COLLABORATIVE RESEARCH BETWEEN THE UNIVERSITIES OF CALIFORNIA AT BERKELEY AND RIVERSIDE AND OREGON STATE UNIVERSITY"

FINAL REPORT FOR JANUARY, 2004- JANUARY, 2005
APRIL, 2007

STEPHEN PARK
University of California, Riverside
The Institute of Geophysics and Planetary Physics
Riverside, California 92521
(909)-787-4501;(909)-787-4324(fax)
magneto@ucrmt.ucr.edu

Submitted to:

UNITED STATES DEPARTMENT OF THE INTERIOR
GEOLOGICAL SURVEY
NATIONAL EARTHQUAKE HAZARDS REDUCTION PROGRAM

Grant 04HQGR0061

Abstract

Since 1988, continuous measurements of natural electrical currents (telluric currents) have been made in Parkfield in order to detect relative changes of resistivity of 1% or less over both short (days) and long (years) term periods. Small changes of resistivity prior to rock failure, well documented in laboratory measurements, will rearrange the distribution of telluric currents. This rearrangment will manifest itself in changes in telluric coefficients relating electric field strength between dipoles. Fractional changes in these coefficients are computed daily and then compared to the time of local earthquake. Previous work has shown that it is unlikely that changes greater than 0.1% are associated with earthquakes with ML<5.0. In September 2004, Parkfield had a M6.0 earthquake followed by two M5 aftershocks. Our initial examination of the telluric coefficients revealed that no significant changes had occurred in the telluric coefficients. We then examined the raw time series in greater detail and found that there was a coseismic voltage transient associated with the main shock and two M5 aftershocks. No other transient signals were seen with the smaller aftershocks. A plausible mechanism for these transient signals is fluid flow generating an electrokinetic signal. The signals are very small, less than 3 mV, and are not unique to the earthquakes. This is not surprising because the telluric analysis cancels out all of the correlated signal, leaving a residual signal containing noise and potential tectonic voltages.

Introduction

Transient electrical signals associated with mechanical disturbances are generally attributed to piezoelectricity or to electrokinetic effects of fluid flow through a porous medium. We eliminate the piezoelectric source because the transient signals persist for up to 8 hours for the main shock; a fluid diffusion process is more consistent with this time period. As explained in the attached manuscript, the signals can be attributed to fluid flow inward towards the fault. This result is consistent with dilatation along the fault and a drop in water well level adjacent to fault.

Data Availability

Time series data and processed results are available via anonymous ftp from vortex.ucr.edu (138.23.185.132) in pub/pkfld. Data from 1988-2004 are presently available. Time series data from 1998-present are also available from the Northern California Earthquake Data Center at UC Berkeley.

Conclusions

Transient coseismic electrical signals were seen with the M6 main shock and two M5 aftershocks in 2004. No smaller aftershock produced measurable signals. These signals were approximately 100 times smaller than the background telluric fluctuations and require careful analysis to extract the transients. Because the analysis involves removing the portion of the signal in a dipole that is correlated with others, the remainder contains noise and any tectonic signals. In the absence of the coincidence with the onset of ground shaking, it is unlikely that the transient tectonic signals could be distinguished from noise. Similar transient signals occur approximately daily in a retrospective analysis of September 2003 (with no earthquakes) and September 2004 (with the M6 earthquake).

2004 Parkfield Earthquake Tests Electromagnetic Precursor Hypothesis

Stephen K. Park, William Dalrymple, Jimmy C. Larsen
Institute of Geophysics and Planetary Physics
University of California, Riverside

Submitted to J. Geophys. Res.
November, 2005
Revised: September 22, 2006
Revised: November 29, 2006

Abstract

A controversy has existed for 30 years concerning the possibility of earthquake prediction using electromagnetic precursors. Long term electromagnetic monitoring prior to, during, and after the M6.0 earthquake at Parkfield, California on 28 September 2004 now provides a definitive test of this hypothesis. During the earthquake our instruments recorded clearly documented electrical signals from an earthquake – impulsive changes of up to +2.5 mV at an electrode located 250 m from the rupture zone followed by a transient decay lasting at least 3 ¼ hours. Similar signals (-1.5 mV) were recorded with the only two M>5 aftershocks, but their transient decays lasted for only ~17 minutes. These signals are unambiguously a result of the earthquake and can be useful in studies of fluid flow in faults, a major current topic in earthquake physics. Patterns in the distribution of transient voltages differ from static stress changes, but are consistent with a small coseismic pressure drop on the fault and fluid flow inward. Signals at a distance of 1 km from the fault are less than 1 mV and are statistically no different from zero in our analysis. Transient voltages for the aftershocks have opposite polarity from those recorded with the main shock and are again maximal close to the fault, suggesting subsequent outward flow from the fault. Finally, there is no evidence of any precursory

signal, strongly calling into question previously suggested signals preceding smaller or more distant earthquakes.

Introduction

Despite over three decades of multinational research, examples of geoelectric signals associated with earthquakes are rare [*Park et al.*, 1993; *Johnston*, 1997], in part because earthquakes potentially large enough to create them are infrequent. Rock samples undergoing strain in laboratory studies show clear signals prior to and during failure that are associated with fluids and piezoelectricity, but field observations are equivocal [*Park et al.*, 1993; *Johnston*, 1997]. If the laboratory measurements are indicative of processes in the Earth, then additional constraints are that the largest strain change (the earthquake) should produce the largest geoelectrical signal and that the signal strength should decay with distance from the hypocenter. One of the more controversial [*Geller et al.*, 1996] experiments in Greece [*Varotsos and Alexopoulos*, 1984] has led to claims of precursory, but not coseismic, changes in electric potentials. Additionally, anthropogenic sources of these signals have been identified [*Pham et al.*, 2003], raising questions of whether the purported precursors are even tectonic in origin. Changes in electric potential were reported prior to M2.4 and M5.0 earthquakes in central California [*Corwin and Morrison*, 1977], but not at the times of the earthquakes. Given the plethora of anthropogenic (e.g., arc welders, electrical grounds, electric fences, water well pumps) and natural (e.g., uptake of water by plant roots, artesian streams, geothermal systems, geomagnetic field variations) sources capable of changing the Earth's electric potential, identification of tectonically-induced potential changes seems exceedingly difficult. The many reported precursory changes in electric potential with no corresponding coseismic

signal thus either contradict extrapolations from laboratory behavior or have resulted from other sources unrelated to tectonic changes.

Telluric Array

We have operated an array (Figure 1) on the San Andreas fault in Parkfield, California since 1988 that is designed to detect variations of the Earth's apparent resistivity [*Park*, 1991]. This array is part of the Parkfield Prediction Experiment [*Roeloffs and Langbein*, 1994]. Every 30 seconds, the array records the electrical potential difference on eight dipoles electronically constructed from five low noise Pb-$PbCl_2$ electrodes (Figure 1). Analog, 2-pole Bessel filters with a –3dB point at 300 s remove shorter period signals, and data are digitally bandpass filtered between 300-7200 s before processing.

Natural variations in the geomagnetic field induce telluric currents that can be measured as time-varying electric potentials on grounded dipoles such as the ones in our array. The telluric currents are modified by the resistivity structure of the Earth, just as current flowing through as series-parallel circuit is partitioned into different branches determined by the values of the resistors. Changing the resistivity of a section of the Earth will alter the distribution of the telluric currents, which can then be observed as changes in electric potential measured on the dipoles.

The telluric method is based on simultaneously recording the electric fields at two sites and then computing the transfer function between these two fields. The relationship between the vector electric field ($\underline{\boldsymbol{E}}_1$) and vector magnetic field ($\underline{\boldsymbol{H}}_1$) at one site is given by the magnetotelluric impedance tensor ($\underline{\underline{\boldsymbol{Z}}}_1$): $\underline{\boldsymbol{E}}_1 = \underline{\underline{\boldsymbol{Z}}}_1 \, \underline{\boldsymbol{H}}_1$. The impedance tensor

contains information about the response of the Earth to the source magnetic field and therefore the resistivity structure. Because the wavelengths of the geomagnetic field are typically much larger than the distance between two sites, we can make the assumption that magnetic field at one site ($\underline{\boldsymbol{H}}_1$) is the same as that at the second site ($\underline{\boldsymbol{H}}_2 \approx \underline{\boldsymbol{H}}_1$). Under this assumption, the relationship between the electric fields at two sites ($\underline{\boldsymbol{E}}_1$, $\underline{\boldsymbol{E}}_2$) is:

$$\underline{\boldsymbol{E}}_2 = \underline{\underline{\boldsymbol{Z}}}_2 (\underline{\underline{\boldsymbol{Z}}}_1)^{-1} \underline{\boldsymbol{E}}_1 = \underline{\underline{\boldsymbol{T}}}_{12} \underline{\boldsymbol{E}}_1, \qquad (1)$$

where $\underline{\underline{\boldsymbol{T}}}_{12}$ is the telluric transfer function. If a change in Earth resistivity occurs, then the telluric transfer function will also change. Normally, electric fields (in V/m) are computed by dividing the electric potential difference on a dipole by its length. We do not use electric fields in our analysis, but rather the potential differences, because the purpose of this study is to look for *changes* in transfer functions and not the functions themselves and because the dipole geometry does not change. The effect of this difference is to incorporate dipole lengths into the telluric transfer function in (1); these could be removed later if desired. For more details on the transfer function analysis, see *Park* [1991].

The largest signal on a dipole results from the telluric currents, and this signal is highly coherent between the multiple dipoles in Figure 1. The dipole signals also contain noise from various sources including electrodes, telephone lines (which are used to connect the electrodes to a central recording location), and circuitry, as well as transient voltages that may be related to anthropomorphic causes and tectonic processes. The telluric transfer function is estimated daily using robust processing [*Park*, 1991], which is a form of cross-correlation analysis coupled with outlier rejection in the time domain. It is based on the correlated, or coherent, part of the signal and rejects the uncorrelated part.

Historically [*Park*, 1991; 1997] we have used dipoles 7 (Lc-Hr) and 8 (Tf-Hr) as references (*Park*, 1991) because these were orthogonal to one another and because they are parallel and perpendicular, respectively, to the San Andreas fault (Figure 1). The choice of reference pair is not important for monitoring as long as the same pair is used throughout the years. Here, we will use three different pairs of references in order to assess the robustness of the transient signals, as is discussed below. The important point about this analysis is that the transfer functions are based on the signal that is correlated between the dipoles (i.e., the telluric currents) and uncorrelated signals are rejected. We will refer here to the uncorrelated signal as the residual signal. Within the residual signal are excursions from background noise levels with durations of less than 24 hours (the increment of time for one estimate of the transfer function) that we will refer to as transient signals.

Data are processed in daily blocks of 2880 points, and transfer function estimates are rejected if coherencies (a measure of the cross-correlation) between the observed signals and the predicted signals using the telluric transfer functions with dipoles 7 and 8 are less than 0.998 (equivalent to a fractional noise of 6%). Coherencies on the day of the 28 September 2004 earthquake were all above 0.999 except for Lc-Hr (0.997) and Tf-Hr (0.995); coherencies computed using the other two of reference dipole pairs (Lc-Hq, Lc-Tf; and Lc-Hq, Tf-Hr) were similar.

Because the primary purpose of the array was to monitor changes in Earth resistivity with precisions appoaching 0.1% [*Park*, 1991; *Madden, LaTorraca, and Park*, 1993; *Park,* 1997], we focused our attention in the past on the transfer functions and therefore the correlated part of the signal. Given the difficulty of unambiguously

separating transient signals due to tectonic causes from those due to noise, the transient signals were never a goal of our study. However, the renewed interest in transient signals purportedly due to tectonic causes [e.g., *Geller, VAN special issue of Geophysical Research Letters*, 1996] and the occurrence of the M6.0 Parkfield earthquake led us to examine our data more closely.

Residual Signals

The component of the electric field measured with one dipole in our array can be written as the linear combination of those measured on two reference dipoles plus a residual signal, $R_i(t)$:

$$D_i(t) = x\, D_{ref\,A}(t) + y D_{ref\,B}(t) + R_i(t). \qquad (2)$$

x and y are the coefficients of the telluric transfer function, $D_{ref\,A}$(t) and $D_{ref\,B}$(t) are the reference signals, and $D_i(t)$ is the signal on one of the other six dipoles in Figure 1. $R_i(t)$ is the component of the signal that is uncorrelated with the reference signals. This residual signal contains all of the noise as well as any transient signals from tectonic causes. A resistivity change caused by stress or strain or new fracture networks opening on the fault would manifest itself in a change in transfer function because it is the resistivity structure that alters the distribution of telluric currents, or the correlated part of the signal. Transient effects such as pressure-induced fluid flow or piezoelectricity would appear in the residual signal unless they, too, were correlated between dipoles.

Residual signals at the time of the earthquake show clear impulsive coseismic transients lasting at least 3 ¼ hours, best shown in the dipole difference Ff-Hq (Figure 2). We show examples of residuals using dipoles 2 (Lc-Hq) and 5 (Lc-Tf) as reference

signals, but we also computed residuals with two other pairs of reference signals in order to verify that the residual signals were not an artifact of reference selection. The other two reference pairs were dipoles 7 (Ff-Hr) and 8(Tf-Hr) and dipoles 1(Lc-Hq) and 8(Tf-Hr). Only this latter reference pair shares no common electrode.

A more complicated behavior is seen on dipoles using Hr, with steps in electric potential occurring as long as 8 ½ hours after the earthquake (Figure 2). Transients exhibit rise times of 4 minutes, which are comparable to the time constant of the analog filters. However, a duration of several hours is much longer than this time constant and must be due to an Earth signal. The observed transients range in magnitude from 0 to 5.5 mV (Table 1), or about 100 times smaller than the signal due to the geomagnetic field variation.

Quantification of the transient magnitude in Figure 2 is difficult because the coseismic signal is superimposed on the noise. For the main shock, the magnitudes of the step changes were estimated from the difference between averages of the residual signals for 1 hour before and 1 hour after the time of the earthquake. For the two M5.0 aftershocks, the transient was estimated as the difference between an average for 30-60 minutes before the earthquake and the peak ranging from 30 s to 5 minutes after the event. We believe this method of estimating the transient magnitudes to be accurate because the calculated transients and visual estimates from Figure 2 (and residual plots using other references) differed by less than the 0.5 mV uncertainty for the plots. Uncertainties in the numerical estimates of the coseismic signal are estimated to be 0.5 mV for the main shock and 0.1 mV for the aftershocks. The smaller uncertainty for the

transients from aftershocks results from their impulsive nature, as opposed to the step function shape for the main shock (Figure 2).

Each of the residual signals is actually a combination of 3 different dipoles sharing 5 electrodes, so extracting the contributions of the individual electrodes requires solution of simultaneous equations. This process is complicated by the fact that there is considerable redundancy in the array; dipoles share common electrodes. While this redundancy has been useful for quality control [*Park*, 1997], it leads to nonuniqueness when inverting for potentials at individual electrodes. A transient voltage at one electrode will be recorded on 3 or 4 dipoles (Figure 1). Equation (2) can be rewritten for the residual signal as:

$$R_i(t) = D_i(t) - x\, D_{ref\,A}(t) - y D_{ref\,B}(t). \qquad (3)$$

For the first residual signal in Figure 2 (Ff-Hq), substitution of the electrode differences for the reference dipoles 2 and 5 yields:

$$R_{Ff\text{-}Hq}(t) = Ff(t)\text{-}Hq(t) - x_{1,25}\,[Lc(t)\text{-}Hq(t)] \;\; - y_{1,25}\,[Lc(t)\text{-}Tf(t)], \qquad (4)$$

where $x_{1,25}$ and $y_{1,25}$ are the telluric coefficients for dipole 1 using dipoles 2 and 5 as references. Finally, the residual signal given by (4) can be rearranged as a linear combination of contributions from 5 electrodes:

$$R_{Ff\text{-}Hq}(t) = Ff(t) - (x_{1,25} + y_{1,25})\, Lc(t) + y_{1,25}\, Tf(t) + (1+x_{1,25})\, Hq(t). \qquad (5)$$

Similar equations can be developed for residual signals for each of 6 dipoles and each of 3 pairs of reference dipoles (Appendix). As can be seen in (4), a signal on Hq or Tf could be partially cancelled because it would appear as part of the correlated signal in Ff-Hq. For each pair of reference dipoles, a set of equations (5) can be solved for electrode

potentials. Because only potential differences can ever be measured, we use Tf as a zero reference potential because it is farthest from the fault.

This set of equations consists of 6 residual equations (5) and one equation Tf = 0 for a set of 5 unknown potentials (Ff, Lc, Tf, Hr, Hq), so we solve it using least squares analysis. Because all of the transient signals in Table 1 occurred at the same time, the electrode potentials determined independently from each pair of reference dipoles should be identical if the analysis is robust. Initial attempts to solve these systems of equations were very unstable, and a singular value decomposition of the system for each reference pair revealed two zero eigenvalues and 3 significant ones (the least squares system for the electrode potentials has 5 variables). This singularity arises because each electrode is used 3-4 times in dipoles. Addition of a damping constant of 0.1 (8 times smaller than the smallest of the 3 significant eigenvalues) stabilized the solution and led to the results in Table 2.

Transient Electrode Potentials for Main Shock

None of the transient electrode potentials exceeded a magnitude of 2.5 mV, while the rms errors ranged from 0.4 mV for dipoles 7 and 8 as references to 0.82 mV with references 1 and 8 (Table 2). If the rms error is used as a proxy for the uncertainty for each electrode potential, none of the potentials determined using the three reference pairs differs significantly from one another. More important is that the signs of the potentials at each electrode are consistent between the analyses with different references (Table 2). Hq always shows the largest magnitude and is positive. The next largest potential is at Hr and it is negative (Table 2). Ff and Lc both show smaller but still negative potentials.

In summary, the results for the main shock indicate a large positive transient potential at Hq and smaller negative potentials at Ff, Lc, and Hr (Figure 1).

Electrode Potentials for M5 aftershocks

Clear transients occurred at the times of the M5.0 aftershocks (17:10:04 on 29 Sept. and 18:54:29 on 30 Sept.), but these were generally impulsive in nature (Figure 2) for residuals determined with all three sets of reference dipoles. Maximum magnitudes of 3.98 mV were observed (Table 3). While these coseismic transient signals were smaller than those for the main shock by factors of 2-3 (compare Tables 1 and 3), this reduction in size was much smaller than the 31 fold difference in seismic moments. Thus, it is clear that these transient signals do not scale with earthquake moment. One of the more obvious differences between the main shock and the aftershocks is that the polarities of the transients are opposite; dipoles that recorded positive transients for the main shock showed negative ones for the aftershocks (Hr-Hq, Figure 2, for example). As will be seen below, this change of polarity will be important when considering mechanisms of generating transients.

Solutions for electrode potentials for the aftershocks on 29 September and 30 September reveal that the peak magnitudes of the potentials are almost as large (Table 4), with a maximum magnitude of 1.50 mV versus 2.51 mV for the M6.0 main shock. Rms errors were more variable for the aftershock solutions however, with values ranging from 0.14 mV using reference dipoles 2 and 5 to 0.97 mV using reference dipoles 7 and 8 (Table 4). Like the main shock, the electrode potentials for the different reference dipoles do not differ significantly from each other if the rms errors are considered (Table

4). With the exception of the potential for Ff for the 29 September aftershock, there is a consistency in signs with different reference dipoles. Electrodes Ff, Lc, and Hr all showed positive potentials, while Hq had a negative change in potential (Table 4). This pattern of electrode polarity is exactly opposite what was seen for the main shock where Hq went positive and the other electrodes went negative. The largest potentials were again at Hq near the fault, and smaller potentials were observed at the more distant electrodes (Ff, Hr, and Lc). Because the rms errors at Ff, Hr, and Lc were generally larger than the magnitudes of the potentials, only the potential at Hr was consistently significant independent of reference dipoles.

Uniqueness of Potential Changes

This pattern of coseismic electric potential changes with both the main shock and the two aftershocks is intriguing, but how diagnostic of earthquakes are they? Examination of the residual signals for a period of one month prior to the earthquake and for an identical period in 2003 (with no earthquake) reveals an average of one impulsive transient with decay times of minutes to hours occurred each day (25 in September 2003 and 27 in September 2004). Additionally, multiple transients were observed and identified as noise spikes because they have time decays comparable to the duration of the impulse response of the filter. Examination of residuals following 28 September 2004 shows barely detectable transients for the two M5.0 aftershocks on 29 September (Figure 2) and 30 September and no changes for any of the smaller aftershocks. Further, retrospective analysis of the residuals shows no transient signals for the five earthquakes with M>4.0 between 1988-2003 (Figure 1). While the large number of transients in 2003

and 2004 is disappointing, we note that only one of these, approximately 9 days prior to the earthquake, had precisely the same polarities as the coseismic signals on 28, 29, and 30 September. This polarity pattern is recognized in the residual signals by transient signals of the same sign on Ff-Hq, Hr-Hq, Ff-Lc, and Hr-Ff, coupled with a change of opposite sign on Tf-Hr (Table 1) and negligible change on Tf-Hq, and is rare among the transient signals observed.

Further, the aftershocks on 29 and 30 September generated transients on dipoles that were *opposite* in sign from those generated by the main shock (Figure 2). Polarity may be diagnostic of tectonic activity, but our existing data are insufficient to confirm this. While impulsive transients may be generated by smaller earthquakes, an earthquake with minimum magnitude of 5 is needed for detection with our array.

Discussion

Piezoelectricity and electrokinetic phenomena are the two most commonly cited causes for transient electric potentials; both have been verified repeatedly in laboratory studies [*Yoshida et al.,* 1997, 1998; *Neishtadt*, 2006; *Eccles et al.*, 2005]. Given the duration of our transient potentials, it is unlikely that they are piezoelectric in origin. The relaxation time for rocks with a resistivity of 100 ohm-m (an upper limit of resistivities observed in the Parkfield region along the fault) is approximately a nanosecond. Even on dry laboratory samples of quartz-rich granite, decay times of only a few seconds are observed [*Yoshida et al.,* 1997] and *Yoshida et al*. [1998] found that the electrokinetic voltage was dominant in wet samples. This dominance was again observed by *Eccles et al.* [2005]. The more probable explanation is that the transient signals are electrokinetic

in origin. Generation of transient electrokinetic potentials (i.e., streaming potentials) associated with fluid flow prior to earthquakes has long been hypothesized [*Fitterman,* 1979]. Electric potentials are generated to counteract charge transfer and separation by bulk flow of an ionic fluid through a negatively charged silicate matrix that preferentially attracts cations [*Morgan et al.,* 1981]. While electrodes need not be located within the flowing fluid to detect such differences, they must be close because the generally conductive rocks in Parkfield [*Park and Fitterman,* 1990] would dissipate electrical current over short distances.

The pattern of a positive potential close to the fault and smaller negative potentials away from the fault can be explained with a model of fluid flow moving towards the fault from the surrounding rocks because potential and pressure gradients are in the opposite direction for electrokinetic potentials [*Morgan et al.*, 1981]. While we also considered a conceptual model with fluid flow emanating from the hypocentral region to the south, the distribution of electrode potentials does not match the expected pattern of the largest potential at Hr and smaller values at increasing distances from the hypocenter (Figure 1). Fluid flow inward towards the fault is also consistent with a water level drop at a monitoring well located just east of the fault and about 500 m from Hq [*Johnston et al.*, 2006].

Another possibility is that permanent compression and dilatation caused by the finite slip on the earthquake created sources and sinks of fluid flow, and rearrangement of the fluid led to transient electric potentials. Comparison of the distribution of the potentials to static stress changes predicted from the slip shows inconsistencies, however (Figure 3). We modeled the earthquake as a patch of uniform slip distributed over the

rupture zone presented by *Langbein et al.* [2005]. This rupture zone extended for 20 km along the fault from the hypocenter northward and extended to a depth of 9 km (Figure 3). Using the observed moment magnitude of 10^{18} Nm [*Langbein et al.*, 2005] and a shear modulus of $3x10^{10}$ N/m^2, we compute the uniform slip on this plane of 0.18 m. A dislocation model [*Okada*, 1972] of the slip shows that electrode Ff is located in a region of compression, electrodes Hr and Lc are in regions of dilatation, and Hq is approximately on a nodal plane (Figure 3). If the voltages were caused simply by the static stress changes, then we would expect regions of compression to have positive potentials, regions of dilatation to have negative potentials, and nodal planes to have no potential. Instead, Hq had a large positive potential and the others had smaller negative potentials. This discrepancy between the observed and expected patterns argues against a causative connection to static stress change.

A potentially troubling aspect of observed potentials is that our signals developed very rapidly relative to the diffusion times of groundwater. While an instantaneous coseismic potential is indistinguishable from a rise over 60-120 seconds because of our low pass filter, pump tests in water wells show drawdown and recovery times are hours, not minutes [*Freeze and Cherry*, 1979]. The signal at Hq is likely not a result of the passage of a pressure pulse at the electrode that caused localized fluid flow but instead resulted from fluid flow at the fault. The recovery time of the signal (3-4 hours) is consistent with the hydrologic response to a transient pressure change, however. The observed transients for Ff-Hq (Figure 2) can be fit using a decaying exponential function with a time constant of ~3000 s for the main shock and ~180 s for the M5.0 aftershock.

This time constant for the main shock is similar to those found associated with the appearance of new hot springs after the San Simeon earthquake [*Wang et al.*, 2004].

The variation of the electrode potential with distance from the fault at the 5 electrodes shows that the largest values occur within 1 km of the fault (Figure 4). The potentials beyond 1000 m from the fault are statistically indistinguishable from 0 mV, so all we can say is that the rupture created a small positive potential on the fault. This positive potential is consistent with fluid flow towards the fault.

Quantification of the pressure gradient that produced the observed potentials is difficult because we have no estimates of the cross-coupling coefficients relating electric potential to the pressure gradient [*Jouniaux and Pozzi,* 1995] for the formations in Parkfield. These coefficients depend on the electrical conductivity of the pore-filling solution, the electric potential between the fluid and silicate mineral (zeta potential), dielectric permittivity of the fluid, and the viscosity of the fluid [*Jouniaux and Pozzi*, 1995]. Further, the potentials are generated only at gradients in these coefficients [*Fitterman,* 1979] and knowledge of the detailed structure is needed to predict how far from the electrodes are these contrasts. Lastly, the relatively conductive rocks in Parkfield will attenuate the signal generated at the fault, thus reducing the potential observed at electrode Hq. However, we can make some assumptions and try to estimate the pressure change.

The electrokinetic potential arises because charge separation caused by fluid flow is countered by a return electrical current called the convection current [*Yoshida,* 2001]. If we assume that the convection current (I_c) is can be treated as a point current source in a homogeneous halfspace of resistivity ρ, then the potential (ϕ) at a distance r generated

by this point source is given by $\phi = \rho I_c / 2\pi r$, and the potential difference between two electrodes at distances r_1 and r_2 is:

$$\Delta\phi = \frac{\rho I_c}{2\pi r_1} - \frac{\rho I_c}{2\pi r_2}. \qquad \textbf{(6)}$$

Electrode Hq is 250 m from the fault, while Hr is 950 m from the fault. If we use a potential difference of ~3.5 mV between these two electrodes (Table 1) and an average resistivity of 60 ohm-m [*Park and Fitterman,* 1990], the convection current at a point source on the fault is 124 mA. If this current were distributed over a surface of 40,000 m^2 (a square patch with a side comparable to the distance between electrode Hq and the fault, we would have a current density of only 3 $\mu A/m^2$; larger patches would reduce the current density further. This current density is comparable to current densities measured in the laboratory in response to a 1 MPa/m pressure gradient perpendicular to the fault [*Yoshida,* 2001].

In reality, the convection currents are likely distributed over the much larger rupture zone and are not uniform but instead mirror the uneven slip distribution [*Langbein, et al.,* 2005]. The actual resistivity and cross-coupling structure are also heterogeneous and can lead to current sources at locations other than the fault. Finally, the electrodes are located adjacent to different segments of the fault and we have assumed a single, common source for all of them. Thus, the 1 MPa/m gradient is probably an overestimate of the actual gradient.

One puzzling aspect of these results is the change in polarity seen for the two M5 aftershocks as compared to the main shock. Potentials were smaller but more significantly, had opposite signs. With positive potentials off the fault and a negative potential at electrode Hq, the reasoning used above would predict fluid flow *away from*

the fault for the aftershocks. A possible explanation is that the main shock resulted in creation of new void space along the fault and the subsequent aftershocks decreased that void space. The drop in water level observed by *Johnston et al.* [2006] is accompanied by a gradual recovery to pre-earthquake levels, although steps are not seen at the times of the two M5.0 aftershocks.

Transient ground water flow has been linked to passage of seismic waves, but is unlikely to have caused our signals. *Brodsky et al.* [2003] and *Wang et al.* [2004] suggest that the seismic wave rearranges mineral particles in the pores of rocks, temporarily increasing permeability and fluid flow. Such a mechanism would likely not account for the sign change between the main shock and aftershock because the waves would increase permeability regardless of the polarity of the ground motion.

Conclusions

A monitoring array has recorded clear coseismic transient electric signals that we attribute to electrokinetic potentials generated by fluid flow. Disappointingly, no precursory signals were detected. The transient signals are also not rare; analyses of data show that such transients occur an average of once per day with no accompanying earthquake or other tectonic changes. Magnitudes, polarities, and decay times of the observed potentials are consistent with a coseismic pressure decrease on the fault followed by hydrologic diffusion of the fluid inward (Figure 1). The spatial distribution of the coseismic electrode potentials precludes a source at the earthquake hypocenter; the maximum potential was observed at an electrode adjacent to the fault, the electrode closest to the hypocenter did not have the largest signal, and potentials elsewhere were

independent of distance from the hypocenter. A retrospective search of data since 1988 reveals that earthquakes with magnitudes less than 5 do not produce significant transient signals, so only infrequent larger earthquakes are likely to generate the them. Monitoring transient electric potentials in the future can benefit studies of the role of fluids in fault zones but will likely not be useful in earthquake prediction. Signals are largest close to the fault (a few mV) and decay to values of less than 1 mV at distances of ~ 1 km. The small electric potential change recorded in the immediate vicinity of a M6.0 earthquake also raises questions about many reports of much larger potentials from smaller and/or more distant earthquakes.

Appendix

Here, we present the full system of equations solved for each of the three pairs of reference dipoles. In the following, $x_{j,25}$ and $y_{j,25}$ are the telluric coefficients for dipole j using dipoles 2 and 5 as references. The second two numbers refer to the reference dipoles. For reference dipoles 2 (Ff-Hq) and 5(Lc-Tf), the other equations are:

$$R_{Tf\text{-}Hq}(t) = -(x_{3,25} + y_{3,25})\,Lc(t) + (1+y_{1,25})\,Tf(t) + (-1+x_{3,25})\,Hq(t), \quad \text{(A1)}$$

$$R_{Hr\text{-}Hq}(t) = -(x_{4,25} + y_{4,25})\,Lc(t) + y_{4,25}\,Tf(t) + Hr(t) + (-1+x_{4,25})\,Hq(t), \quad \text{(A2)}$$

$$R_{Ff\text{-}Lc}(t) = Ff(t) - (1 + x_{6,25} + y_{6,25})\,Lc(t) + y_{6,25}\,Tf(t) + x_{6,25}\,Hq(t), \quad \text{(A3)}$$

$$R_{Hr\text{-}Ff}(t) = -Ff(t) - (x_{7,25} + y_{7,25})\,Lc(t) + y_{7,25}\,Tf(t) + Hr(t) + x_{7,25}\,Hq(t), \quad \text{(A4)}$$

and

$$R_{Tf\text{-}Hr}(t) = -(x_{8,25} + y_{8,25})\,Lc(t) + (1+y_{1,25})\,Tf(t) - Hr(t) + x_{8,25}\,Hq(t). \quad \text{(A5)}$$

For reference dipoles 7(Hr-Ff) and 8(Tf-Hr), the equations are:

$$R_{Ff\text{-}Hq}(t) = (1 + x_{1,78})Ff(t) - y_{1,78}\,Tf(t) + (-x_{1,78} + y_{1,78})\,Hr(t) - Hq(t), \quad \text{(A6)}$$

$$R_{Lc\text{-}Hq}(t) = x_{2,78}\,Ff(t) + Lc(t) - y_{2,78}\,Tf(t) + (-x_{2,78} + y_{2,78})\,Hr(t) - Hq(t), \quad \text{(A7)}$$

$$R_{Tf\text{-}Hq}(t) = x_{3,78}\,Ff(t) + (1 - y_{3,78})Tf(t) + (-x_{3,78} + y_{3,78})\,Hr(t) - Hq(t), \quad \text{(A8)}$$

$$R_{Hr\text{-}Hq}(t) = x_{4,78}\,Ff(t) - y_{4,78}\,Tf(t) + (1 - x_{4,78} + y_{4,78})\,Hr(t) - Hq(t), \quad \text{(A9)}$$

$$R_{Lc\text{-}Tf}(t) = x_{5,78}\,Ff(t) + Lc(t) - (1 + y_{5,78})Tf(t) + (-x_{5,78} + y_{5,78})\,Hr(t), \quad \text{(A10)}$$

and

$$R_{Ff\text{-}Lc}(t) = (1 + x_{6,78})Ff(t) - Lc(t) - y_{6,78}\,Tf(t) + (-x_{6,78} + y_{6,78})\,Hr(t). \quad \text{(A11)}$$

For reference dipoles 1(Ff-Hq) and 8(Tf-Hr), the equations are:

$$R_{Lc\text{-}Hq}(t) = -x_{2,18}\,Ff(t) + Lc(t) - y_{2,18}\,Tf(t) + y_{2,18}\,Hr(t) + (-1 + x_{2,18})\,Hq(t), \quad \text{(A12)}$$

$$R_{Tf\text{-}Hq}(t) = -x_{3,18}\,Ff(t) + (1 - y_{3,18})Tf(t) + y_{3,18}\,Hr(t) + (-1 + x_{3,18})\,Hq(t), \quad \text{(A13)}$$

$$R_{Hr\text{-}Hq}(t) = -x_{4,18}\,Ff(t) - y_{4,18}\,Tf(t) + (1 + y_{4,18})\,Hr(t) + (-1 + x_{4,18})\,Hq(t), \quad \text{(A14)}$$

$$R_{Lc\text{-}Tf}(t) = -x_{5,18}\,Ff(t) + Lc(t) - (1 + y_{5,18})Tf(t) + y_{5,18}\,Hr(t) + x_{5,18}\,Hq(t), \quad \text{(A15)}$$

$$R_{Ff\text{-}Lc}(t) = (1 - x_{6,18})Ff(t) - Lc(t) - y_{6,18}\,Tf(t) + y_{6,18}\,Hr(t) + x_{6,18}\,Hq(t), \quad \text{(A16)}$$

and

$$R_{Hr\text{-}Ff}(t) = -(1 + x_{7,18})\,Ff(t) - y_{7,18}\,Tf(t) + (1 + y_{7,18})\,Hr(t) + x_{7,18}\,Hq(t). \quad \text{(A17)}$$

Acknowledgements

We thank Evelyn Roeloffs and Harry Green for their comments on an earlier draft of this manuscript, and David Oglesby for useful discussions. We offer special thanks to David Fitterman whose question about the difference between references led to the residual analysis presented here. Robert Simpson kindly gave us his dislocation modeling programs based on *Okada* [1992]. This work was supported by the U.S. Geological Survey (USGS), Department of the Interior, under USGS Award numbers 04HQGR0061

and 05HQGHR0036. The views and conclusions contained in this document are those of the authors and should not be interpreted as necessarily representing the official policies, either expressed or implied, of the U.S. Government. Seismic data are from the Northern California Earthquake Data Center operated by the Berkeley Seismological Laboratory.

Table 1. Magnitudes of signals observed on dipoles with different references for main shock on 28 September 2004.

Dipole Number	Dipole	Voltage, mV		
		Ref. 2,5	Ref. 7,8	Ref. 1,8
1	Ff-Hq	-3.62	-2.78	x
2	Lc-Hq	x	-3.62	-1.54
3	Tf-Hq	+0.00	-2.96	-4.77
4	Hr-Hq	-5.34	-2.82	-4.60
5	Lc-Tf	x	-1.30	-4.87
6	Ff-Lc	-3.74	+1.04	+1.49
7	Hr-Ff	-3.32	x	-4.57
8	Tf-Hr	+5.48	x	x

Table 2. Changes in electrode potentials for main shock on 28 September 2004. Numbers statistically different from 0 mV are in bold.

Electrode	Potential, mV		
	Ref. 2,5	Ref 7,8	Ref. 1,8
Ff	-0.77	-0.27	-0.40
Lc	-0.41	**-0.74**	-0.62
Tf	-0.04	-0.02	-0.03
Hr	**-0.90**	**-1.08**	**-1.13**
Hq	**+2.51**	**+2.27**	**+2.48**
√rms, mV	0.82	0.40	0.82

.

Table 3. Magnitudes of signals observed on dipoles with different references for two M5 aftershocks.

Dipole Number	29 Sept. M5.0				30 Sept. M5.0		
	Dipole	Voltage, mV			Voltage, mV		
		Ref. 2,5	Ref. 7,8	Ref. 1,8	Ref. 2,5	Ref. 7,8	Ref. 1,8
1	Ff-Hq	+1.09	+1.13	x	+1.17	+0.71	x
2	Lc-Hq	x	+1.31	+0.05	x	+1.38	+1.52
3	Tf-Hq	+0.01	+1.12	+0.74	-0.01	+0.82	+1.48
4	Hr-Hq	+2.16	+3.98	+0.81	+1.86	+0.73	+1.15
5	Lc-Tf	x	+0.27	-0.64	x	+0.43	-1.13
6	Ff-Lc	+1.07	-0.15	-0.11	+1.26	-0.57	-1.45
7	Hr-Ff	+1.13	x	+0.90	+1.33	x	+1.40
8	Tf-Hr	-2.14	x	x	-2.07	x	x

Table 4. Changes in electrode potentials for the two M5 aftershocks. Numbers statistically different from 0 mV are in bold.

	Sept. 29 M5.0			Sept. 30 M5.0		
	Potential, mV			Potential, mV		
Electrode	Ref. 2,5	Ref. 7,8	Ref. 1,8	Ref. 2,5	Ref. 7,8	Ref. 1,8
Ff	**+0.20**	+0.49	+0.12	+0.18	-0.01	-0.17
Lc	**+0.18**	+0.14	+0.04	+0.15	**+0.32**	+0.44
Tf	+0.01	+0.03	+0.01	+0.01	-0.00	-0.01
Hr	**+0.38**	+0.51	+0.14	+0.40	**+0.37**	**+0.63**
Hq	**-0.90**	**-1.50**	**-0.39**	**-0.88**	**-0.65**	**-0.81**
√rms, mV	0.14	0.97	0.22	0.42	0.25	0.61

Fig. 1. Telluric monitoring array in Parkfield showing electrode locations (Ff, Lc, Hq, Tf, Hr). County boundaries are thin black lines, and dipoles are shown in yellow. Lc-Hq and Lc-Tf are used as reference dipoles in the telluric analysis. Focal mechanisms scaled by magnitude are shown at the epicenters of the M6.0 earthquake and the 29 September M5.0 aftershock. The second M5.0 aftershock is shown with a blue square, and other aftershocks are shown with open or solid black circles. Pink squares mark locations of past M>4 earthquakes since 1988. Coseismic electrode potentials are shown with red (positive) or blue (negative) dots scaled by the magnitude of the potential; see text for discussion. The largest change of 2.51 mV is at Hq.

Fig. 2. Residual signals at the time of the M6.0 earthquake and the two M5.0 aftershocks. Scaled voltages are plotted versus Universal Time between 12:00 on 28 September 2004 and 04:00 on 29 September 2004. The separate plots to the right shows voltages recorded in a window from 16:00 to 18:00 on 29 September 2004 and in a window from 18:00 to 20:00 on 30 September 2004. The occurrences of the M6.0 earthquake at 17:15 on 28 September, the M5.0 aftershock at 17:10 on 29 September, and the M5.0 aftershock at

18:54 on 30 September are shown. Transient signals are colored pink (negative) or blue (positive) to distinguish them from the residual signals within which they are embedded. Note that no transients are shown for Lc-Hq and Lc-Tf because these were the reference dipoles for the residual analysis. No residual is observed for Tf-Hq because this dipole is identically equal to (Lc-Hq)-(Lc-Tf). Time marks are every 30 minutes with longer lines for hours.

Figure 3 – Electrode potential changes superimposed on dislocation model of M6.0 earthquake. Shaded plane represents slip plane for earthquake. The pattern of dilatation (positive) and compression (negative) is consistent with right lateral strike slip motion on fault. However, Ff, Lc, and Hr all showed negative potentials even though the electrodes experienced both dilatation and compression. Inset box represents extent of dislocation model volume.

Figure 4 – Variation of electrode potential with perpendicular distance from fault. Uncertainties are based on rms errors for solution of potentials. Note how transients are essentially zero beyond 1000 m from the fault.

References

Brodsky, E.E., E. Roeloffs, D. Woodcock, I. Gall, and M. Manga, A mechanism for sustained groundwater pressure changes induced by distant earthquakes, *J. Geophys. Res., 108*, 10.1029/2002JB002321, 2003.

Corwin, R.F. and H.F. Morrison, Self-potential variations preceeding earthquakes in central California, *Geophys. Res. Lett., 4*, 171-174, 1977.

Eccles, D., P.R. Sammonds, and O.C. Clint, Laboratory studies of electric potential during rock failure, *Intl. J. Rock Mech. and Mining Sci., 42*, 933-949, 2005.

Fitterman, D.V., Theory of electrokinetic-magnetic anomalies in a faulted half-space, *J. Geophys. Res., 84*, 6031-6040, 1979.

Freeze, A.R., and J.A. Cherry, *Groundwate*r, Prentice Hall, 604 pp., 1979.

Geller, R.J., Debate on evaluation of the VAN method: Editor's introduction, *Geophys. Res. Lett., 23*, 1291-1293, 1996.

Johnston, M.J.S., Review of electric and magnetic fields accompanying seismic and volcanic activity, *Surv. Geophys., 18*, 441-475, 1997.

Johnston, M.J.S., R.D. Borcherdt, A.T. Linde, and M.T. Gladwyn, Continuous borehole strain and pore pressure in the near field of the 28 September 2004 M 6.0 Parkfield, California, earthquake; implications for nucleation, fault response, earthquake prediction, and tremor, *B. Seism. Soc. Am., 96*, S56-S72, 2006.

Jouniaux, L. and J.P. Pozzi, Streaming potential and permeability of saturated sandstones under triaxial stress: consequences for electrotelluric anomalies prior to earthquakes, *J. Geophys. Res., 100,* 10197-10209, 1995.

Langbein, J., R. Borcherdt, D. Dreger, J. Fletcher, J.L. Hardebeck, M. Hellweg, C. Ji, M. Johnston, J.R. Murray, R. Nadeau, M.J. Rymer, and J.A. Teriman, Preliminary report on the 28 September 2004, M6.0 Parkfield, California earthquake, *Seis. Res. Lttr., 76*, 10-26, 2005.

Madden, T.R., G.A. LaTorraca, and S.K. Park, Electrical conductivity variations around the Palmdale section of the San Andreas fault zone, *J. Geophys. Res., 98*, 795-808, 1993.

Morgan, F.D., E.R. Williams, and T.R. Madden, Streaming potential properties of westerly granite with applications, *J. Geophys. Res., 94*, 12449-12461, 1989.

Neishtadt, N.M., L.V. Eppelbaum, and A.G. Levitski, Application of piezoelectric and seismoelectrokinetic phenomena in exploration geophysics: Review of Russian and Israeli experiences, *Geophys. 71*, B41-B53, 2006.

Okada, Y., Internal deformation due to shear and tensile faults in a half space, *Bull. Seis. Soc. Am., 82*, 1018-1040, 1992.

Pham, V.N., D. Boyer, G. Chouliaras, A. Savvaidis, G. Stavrakakis, and J.L. LeMouel, Sources of anomalous transient electric signals (ATESs) in the ULF band in the Lamia region (central Greece): electrochemical mechanisms for their generation, *Phys. Earth Planet. Int., 130*, 209-233, 2002.

Park, S. K., Monitoring resistivity changes prior to earthquakes in Parkfield, California with telluric arrays: *J. Geophys. Res.*, 96, 14211-14237, 1991.

Park, S.K., Monitoring resistivity changes in Parkfield, California: 1988-1995, *J. Geophys. Res., 102*, 24545-24559, 1997.

Park, S.K. and D.V. Fitterman, Sensitivity of the telluric monitoring array in Parkfield, California to changes of resistivity, *J. Geophys. Res., 95*, 15,557-15,571, 1990.

Park, S.K., M.J.S. Johnston, T.R. Madden, F.D. Morgan, and H.F. Morrison, Electromagnetic precursors to earthquakes in the ulf band: A review of observations and mechanisms, *Rev. Geophys., 31*, 117-132, 1993.

Roeloffs, E.A. and J. Langbein, The earthquake prediction experiment at Parkfield, California, *Rev. Geophys., 32*, 315-336, 1994.

Varotsos, P. and K. Alexopoulos, Physical properties of the variations of the electric field of the earth preceding earthquakes, I, *Tectonophys., 110*, 73-98, 1984.

Wang, C.Y., M. Manga, D. Dreger, and A. Wong, Streamflow increase due to rupturing of hydrothermal reservoirs: evidence from the 2003 San Simeon, California, earthquake, *Geophys. Res. Lett., 31*, 10.1029/2004GL020124, 2004.

Yoshida, S., Convection current generated prior to rupture in saturated rocks, *J. Geophys. Res., 106*, 2103-2120, 2001.

Yoshida, S., O.C. Clint, and P.R. Sammonds, Electric potential changes prior to shear fracture in dry and saturated rocks, *Geophys. Res. Lett., 25*, 1577-1580, 1998.

Yoshida, S., M. Uyeshima, and M. Nakatani, Electric potential changes associated with slip failure of granite: preseismic and coseismic signals, *J. Geophys. Res., 102*, 14883-14897, 1997.

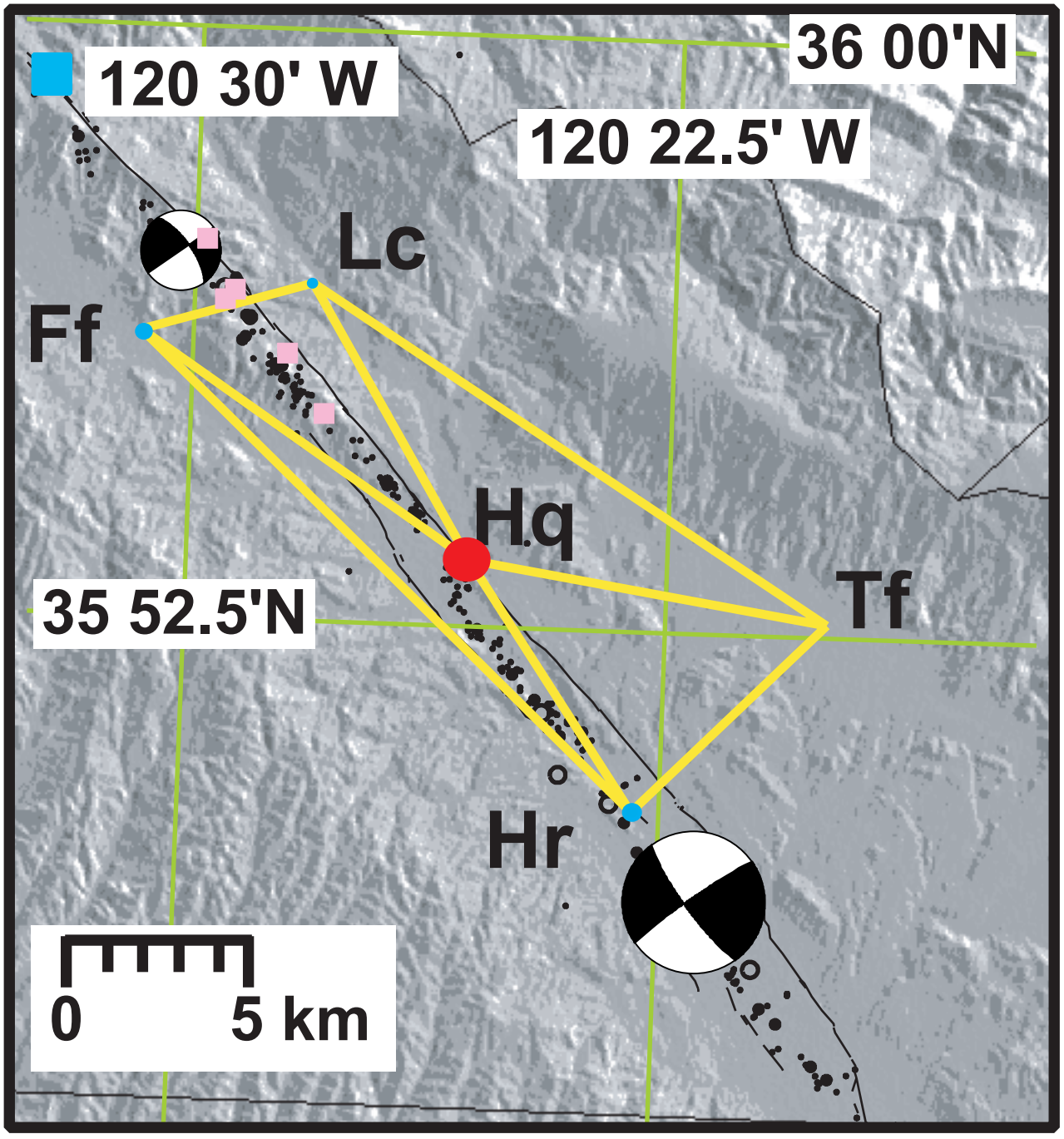

Fig 1

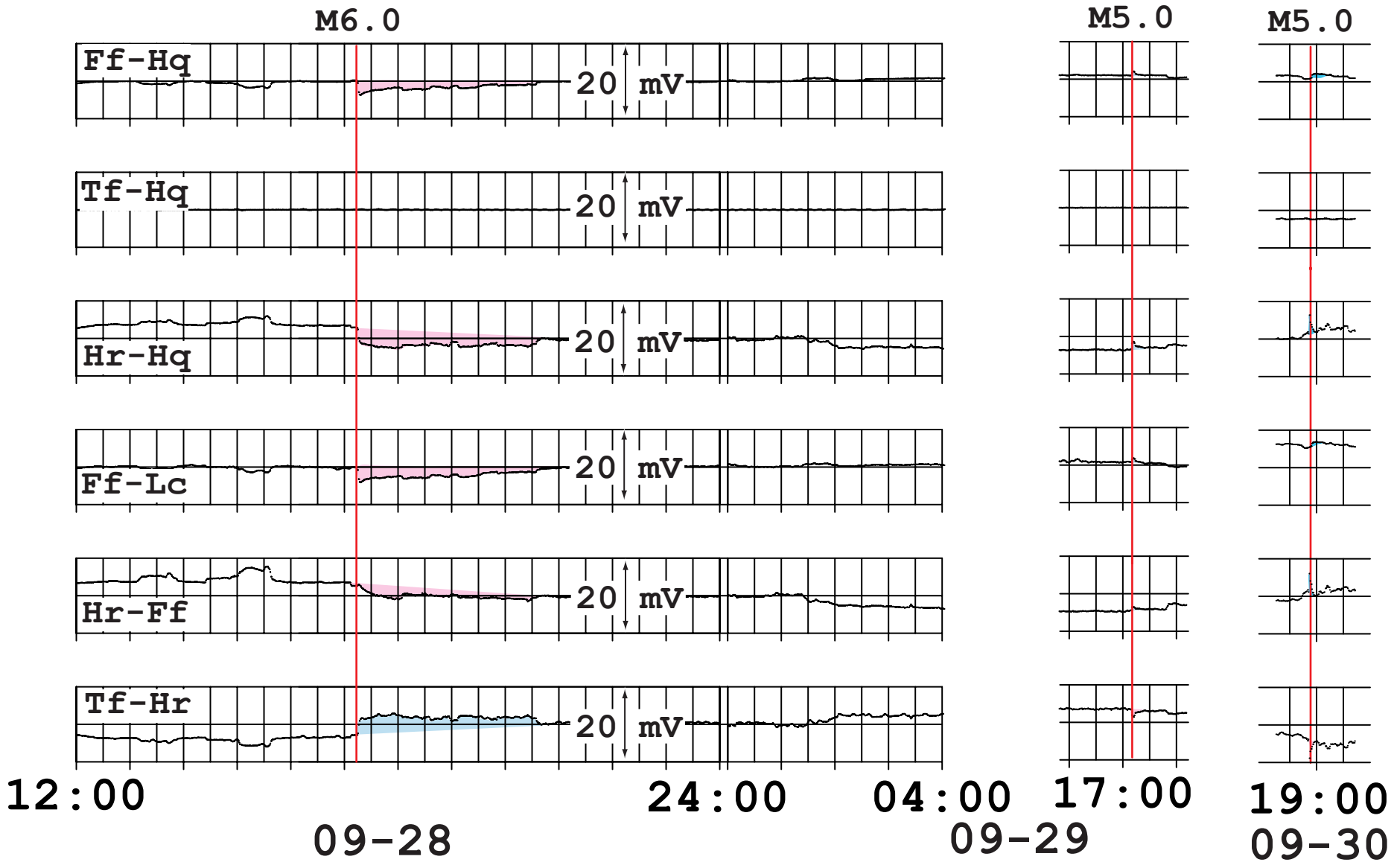
M6.0
M5.0
M5.0
Ff-Hq
Tf-Hq
Hr-Hq
Ff-Lc
Hr-Ff
Tf-Hr
20 mV
12:00
09-28
24:00
04:00
09-29
17:00
19:00
09-30

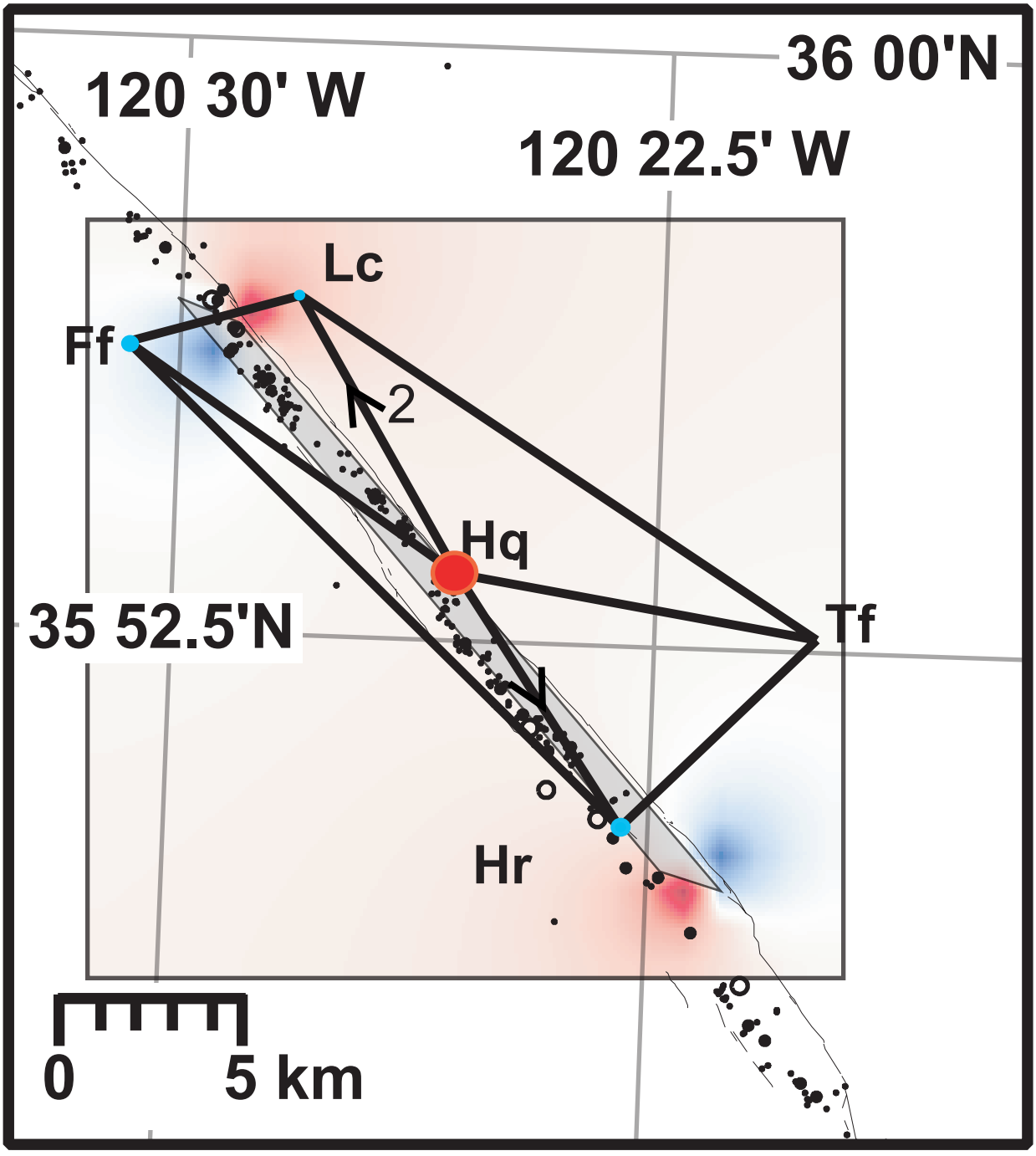
36 00'N
120 30' W
120 22.5' W
Lc
Ff
2
Hq
35 52.5'N
Tf
1
Hr
0
5 km

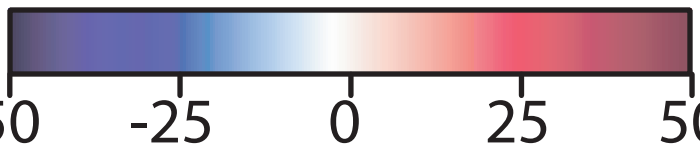
-50
-25
0
25
50
Dilatation, με

Fig 3

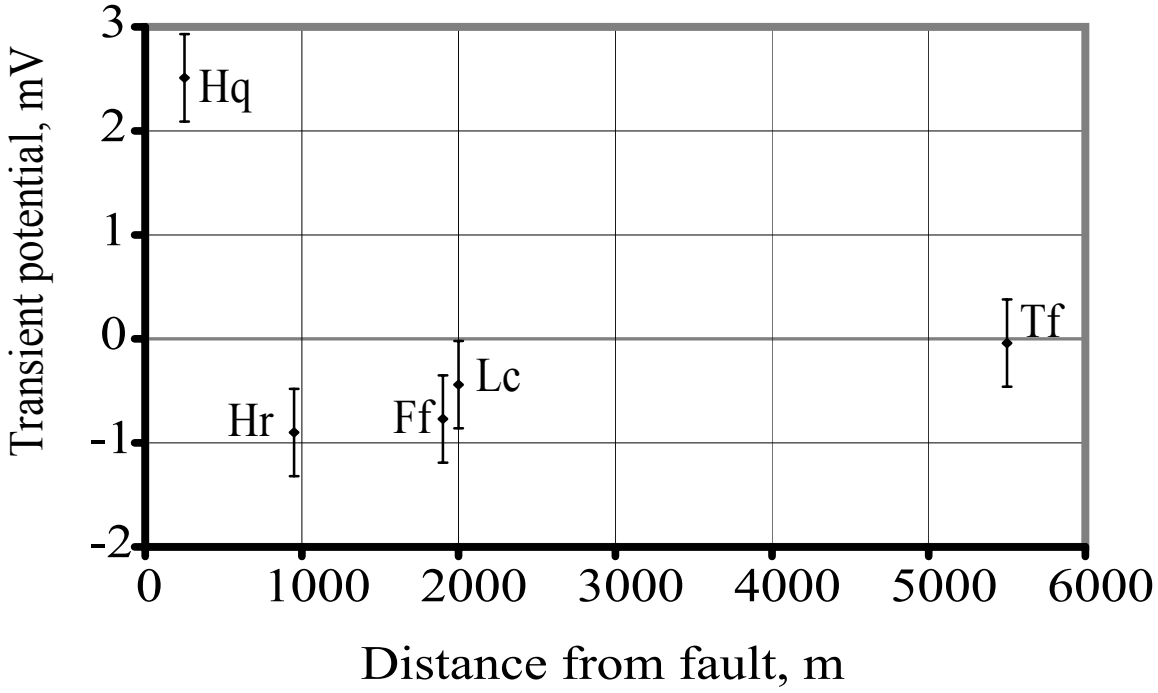
Transient potential, mV
3
2
1
0
-1
-2
Hq
Hr
Ff
Lc
Tf
0
1000
2000
3000
4000
5000
6000
Distance from fault, m

Fig.4